Lattice Boltzmann simulation of nonideal vapor-liquid flow in porous media

A. D. Angelopoulos, V. N. Paunov,* V. N. Burganos, and A. C. Payatakes
Institute of Chemical Engineering and High Temperature Chemical Processes—Foundation for Research and Technology, Hellas, P.O. Box 1414, 26500 Patras, Greece
and Department of Chemical Engineering, University of Patras, 26500 Patras, Greece
(Received 4 June 1997; revised manuscript received 14 October 1997)

A lattice-Boltzmann simulator of two-phase equilibrium and flow is presented and applications to interface stability problems are discussed. The simulator is based on a lattice-Boltzmann model of nonideal fluids that allows coexistence of two phases of a single substance at an explicitly defined temperature. A set of thermodynamically consistent algorithms is developed to prescribe the equilibrium densities and kinematic viscosities of the vapor and liquid phases of a van der Waals fluid and also the interfacial tension and interfacial thickness. Flow is induced by applying either a constant macroscopic pressure gradient or an external body force. Application to gas displacement by liquid in a pore structure showed that the simulator is capable of reproducing critical flooding phenomena under strong wettability conditions, such as formation of thin films, snap-off in narrow throats, and entrapment of the nonwetting phase. [S1063-651X(98)11103-0]

PACS number(s): 47.55.Mh, 44.30.+v, 05.40.+j

I. INTRODUCTION

The hydrodynamic behavior of multiphase systems has been the subject of a large number of theoretical and experimental investigations, not only because of its strong scientific interest but also because of its unusual technological importance, as it is directly connected to a number of modern practical problems and applications, including soil pollution and remediation, enhanced oil recovery, color printing, foaming, emulsion flow and stability, etc. The modeling of multiphase flow processes is an extremely difficult task within the classical hydrodynamics discipline owing, mainly, to the inherent free-boundary complication. For instance, experimental studies [1–3] have shown that during two-phase flow in porous media the nonwetting fluid is usually highly disconnected and exhibits a rich flow behavior that depends on the externally imposed conditions.

The lattice-gas and lattice-Boltzmann methods, which are based on the cellular automaton concept, enjoyed rapid development over the last decade, and provided an interesting alternative to traditional numerical techniques for solving the Navier-Stokes equation (see, e.g., Ref. [4]). These numerical algorithms can easily be implemented on parallel computers and are expected to offer significant advancement in addressing complex hydrodynamic problems. The great advantage of the cellular automata methods is that they can easily simulate fluid flow with highly complex solid or free boundaries. For instance, it has been repeatedly shown in the literature that a lattice-Boltzmann scheme can be easily adapted to simulate flow in porous media, motion of deformable bodies in complex geometries, and multiphase flow under both dynamic and quasistatic conditions. Especially for three-dimensional (3D) problems, the lattice-Boltzmann method is proven to compete with the most advanced spectral methods of the computational hydrodynamics [5]. It is beyond the scope of the present article to review the evolution of the cellular automata techniques and approaches. Rather, mention will be made of those attempts that place particular emphasis on the use of thermodynamic arguments to support the lattice-gas or lattice-Boltzmann description of phase equilibrium, phase transition, and two-phase flow.

In the lattice-gas methods a discrete set of particles moves on discrete space (lattice) in discrete time. The particles undergo collisions at the lattice nodes according to a certain set of collision rules. The lattice-Boltzmann method is a probabilistic equivalent of the lattice-gas method, where the discrete particles are replaced with the respective values of their mean populations. By modifying the equilibrium distributions of the particle populations, the Navier-Stokes equation is recovered at the long-wavelength limit.

In the case of multiphase flow, special care should be taken to ensure stable phase separation. Most of the existing schemes achieve this by employing phenomenological ''antidiffusion'' operators (see, e.g., Ref. [6]). Surface tension is induced by mass perturbation and redistribution algorithms [7–8]. A common weakness of these approaches is that they are based on, practically, arbitrary momentum exchange within the interfacial region, and this produces *significant spurious currents* even at equilibrium. As a consequence, when flow conditions are imposed, the velocity field in the bulk can be strongly perturbed by this exchange of momentum at the interface.

A different line of work was pursued by Appert and coworkers [9–12], who modified the classical lattice-gas model and introduced momentum exchange between remote particles in order to induce phase transition. This interesting approach is implemented through the so-called ''maximal'' and ''minimal'' interaction models. If $\mathbf{g}_a$ and $\mathbf{g}_b$ are the momenta of interacting particles at prespecified distance r from each other, then the new momenta become $\mathbf{g}_a+\mathbf{t}$ and $\mathbf{g}_b-\mathbf{t}$, respectively, where $|\mathbf{t}|$ is the amount of momentum exchanged. In the ''minimal'' model, $\mathbf{g}_a \| \mathbf{g}_b \| \mathbf{t}$. In the ''maximal'' model, the largest possible momentum exchange is implemented among particles that may move in parallel or nonparallel directions, without violating the conservation of particle number or of the total momentum of the interacting

*Permanent address: Faculty of Chemistry, University of Sofia, Sofia, Bulgaria.

ensemble. As the distance between interacting particles exceeds a certain value, a liquid-gas type of phase transition is obtained. However, this approach is not thermodynamically rigorous, the Gibbs-Thomson relations are not verified, and the Galilean invariance issue remains unresolved.

Chen and co-workers have introduced modified lattice-gas [13] and lattice-Boltzmann [14–15] models of phase coexistence for single-component and multicomponent systems based on nearest-neighbor interactions. Detailed analysis of the single-component model has shown that the lattice-Boltzmann variant conserves momentum, and that the density profile in the liquid-gas interface can be expressed in terms of a temperaturelike parameter. The mutual diffusivity in a binary mixture is calculated analytically in terms of the concentrations of the two components and is found to be Galilean invariant. Although computationally efficient and flexible for practical applications, this model could be further improved by restoring sitewise energy conservation and defining temperature in a thermodynamically consistent manner.

Recently, Swift and co-workers [16–19] developed lattice-Boltzmann methods for the modeling of isothermal systems made up of either a vapor and a liquid phase of a single species or two mutually interacting fluids. In both cases, the equilibrium state is associated with a free-energy functional, which, in turn, can be used for the calculation of a pressure tensor, using the Cahn-Hilliard description of nonequilibrium dynamics [20]. In the single-component case [16], a nonideal equation of state for the fluid suffices to ensure phase separation below the critical point. In the binary mixture case, two independent densities are defined, each of which is assumed to evolve according to the usual single-relaxation-time lattice-Boltzmann equation [18]. The thermodynamic aspects of this model are discussed in view of a simple binary-fluid model, namely, two ideal gases with repulsive interaction. These models exhibit largely reduced spurious currents compared to other two-phase models and present reasonable kinetics of the approach to equilibrium.

The present work provides an investigation of the single-component, two-phase lattice-Boltzmann model, developed by Swift, Osborn, and Yeomans [16]. This model deserves special attention and further analysis, because it provides an excellent basis for explicit definition of vapor and liquid phases within the lattice-Boltzmann framework. The chemical potential concept is introduced into this model, and a detailed algorithm for a thermodynamically consistent prescription of the basic equilibrium properties, namely, vapor and liquid densities, interfacial tension, and interface thickness, is presented. By rendering the collision relaxation-time density dependent, the *kinematic viscosities* of the liquid and of the vapor can also be prescribed in an explicit fashion. The Gibbs-Thomson equations are satisfied with good accuracy by our simulation results for a liquid droplet at equilibrium, without having to resort to the employment of a correction factor. In addition, a two-phase flow simulator is developed based on this model, which is capable of predicting the evolution of immiscible displacement processes in porous media. It is shown that this simulator can predict several interesting phenomena associated with displacement processes, such as the formation of a precursor wetting film [1–2], early breakthrough, and snap-off of the nonwetting phase in narrow pores [3]. The combination of these phenomena can be responsible for poor flooding performance and low sweeping efficiency in enhanced oil recovery and soil remediation applications.

II. PRESCRIPTION OF THE FLUID PROPERTIES

A. Equilibrium densities

We show here how the equilibrium densities of the vapor and liquid phases of a nonideal fluid can be prescribed in the context of the lattice-Boltzmann scheme. This is achieved by recovering the respective nonideal equation of state from the conditions of thermodynamic equilibrium in an inhomogeneous system. It is well known from thermodynamics that in order for a liquid and its vapor to coexist at a given temperature, they must share the same pressure and chemical potential:

$$P(\rho_1,T)=P(\rho_2,T)=P_0(T), \tag{1}$$

$$\mu(\rho_1,T)=\mu(\rho_2,T)=\mu_{\mathrm{eq}}(T), \tag{2}$$

where ρ_1 and ρ_2 are the densities of the vapor (gas) and the liquid, respectively, and $\mu_{\mathrm{eq}}(T)$ is the equilibrium chemical potential.

Let us assume that the two phases obey the van der Waals equation of state,

$$P(\rho,T)=\rho kT/(1-b\rho)-a\rho^2, \tag{3}$$

which corresponds to the following expression for the chemical potential:

$$\mu(\rho,T)=kT\,\ln[\rho/(1-b\rho)]+kT/(1-b\rho)-2a\rho. \tag{4}$$

In Eq. (4), kT is the thermal energy, and a and b are the van der Waals constants,

$$b=1/3\rho_c,\quad kT_c=8a/27b, \tag{5}$$

with ρ_c and T_c being the critical density and critical temperature, respectively. At a fixed temperature ($T<T_c$) the two phases can coexist at a single pressure value only, $P_0(T)$, which is determined by the so-called Maxwell construction (equal areas rule) and satisfies Eq. (2). The van der Waals constants can be expressed in terms of the prescribed densities and the temperature in the following form, resulting from algebraic manipulation of Eqs. (1)–(4):

$$b=\frac{2}{\rho_1+\rho_2}-\frac{(1-b\rho_1)(1-b\rho_2)}{\rho_2-\rho_1}\ln\frac{\rho_2(1-b\rho_1)}{\rho_1(1-b\rho_2)}, \tag{6}$$

$$a=\frac{kT}{(\rho_1+\rho_2)(1-b\rho_1)(1-b\rho_2)}. \tag{7}$$

Note that Eq. (6) is a transcendental equation for b that can be solved with no reference to the temperature. Then, from Eqs. (5) and (7) one can estimate how far the system is from the critical state at the prescribed density ratio (Fig. 1):

$$T/T_c=27b(\rho_1+\rho_2)(1-b\rho_1)(1-b\rho_2)/8. \tag{8}$$

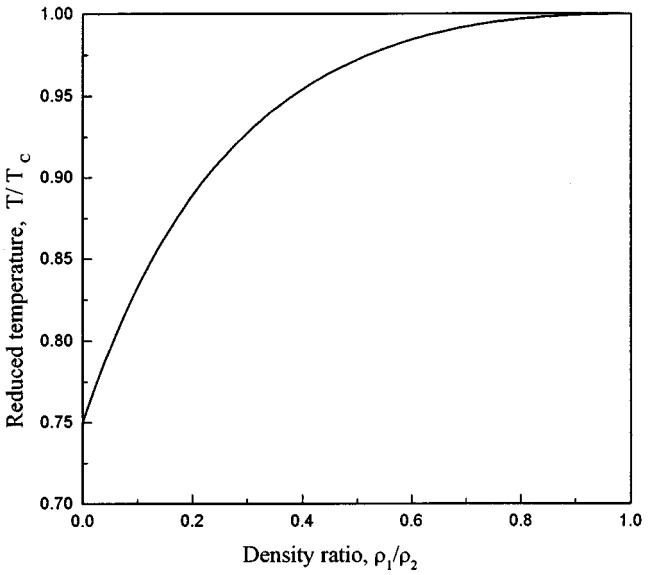

FIG. 1. Dependence of the reduced temperature T/T_c on the density ratio ρ_1/ρ_2 for a van der Waals fluid.

B. Kinematic viscosities

Since the two-phase system is made up of a single component, special care should be taken to prescribe the viscosities of the liquid and the vapor in a consistent manner. This can be accomplished by expressing the kinematic viscosity ν as a linear function of the relaxation time τ of the lattice-Boltzmann collision operator

$$\nu_k=(2\tau_k-1)/8; \quad k=1,2. \tag{9}$$

One can let τ depend on density through a simple expression, such as

$$\tau(\rho)=A\rho+B, \tag{10}$$

under the obvious constraints:

$$\tau(\rho_1)=\tau_1, \quad \tau(\rho_2)=\tau_2. \tag{11}$$

A combination of Eqs. (10) and (11) gives

$$\tau(\rho)=\frac{(\tau_2-\tau_1)\rho+\tau_1\rho_2-\tau_2\rho_1}{\rho_2-\rho_1}. \tag{12}$$

In this way, the two phases (liquid and vapor) can be assigned different kinematic viscosities, ν_1 and ν_2, while maintaining a continuous transition of the local viscosity and of the relaxation constant across the interface.

C. Interfacial tension

According to the van der Waals theory of interfacial tension, the total free-energy functional for a liquid-vapor system has the form

$$F[\rho(\mathbf{r})]=\int d\mathbf{r}[\tfrac{1}{2}m|\nabla\rho(\mathbf{r})|^2+\tilde{\psi}(\rho(\mathbf{r}))], \tag{13}$$

where $\tilde{\psi}$ is the local excess of the free-energy density with respect to the bulk phases, and m is a parameter independent of $\nabla\rho(\mathbf{r})$ and higher-order derivatives. The optimal density distribution $\rho(\mathbf{r})$ that minimizes the free energy of the system is usually found by analogy with classical mechanics (see, e.g., Ref. [20]). Thus, it can be shown, in view of the mean-field approximation, that for a *flat* interface the fluid density across the interface, $\rho(z)$, satisfies the equation

$$m\rho''(z)=\mu(\rho,T)-\mu_{\rm eq}(T), \tag{14}$$

where the local excess of chemical potential can be viewed as an ''external force'' in the mechanical analogue.

Using the assumption that the temperature T is near the critical temperature T_c, the right-hand side of Eq. (14) can be expanded in series around T_c and ρ_c. Then the expression

$$\rho(z)=\rho_c+\tfrac{1}{2}(\rho_2-\rho_1)\tanh(2z/D) \tag{15}$$

satisfies Eq. (14) with good accuracy, where D is a measure of the interface thickness.

Even far from the critical point, it can easily be inferred [using Eqs. (2), (4), and (7)] that the local excess of chemical potential can be written in the form

$$\mu(\rho,T)-\mu_{\rm eq}(T)=kTf(\rho), \tag{16}$$

where

$$f(\rho)=g(\rho)-g(\rho_1)=g(\rho)-g(\rho_2), \tag{17}$$

and

$$g(\rho)=\ln\frac{\rho}{1-b\rho}+\frac{1}{1-b\rho}-\frac{2\rho}{(\rho_1+\rho_2)(1-b\rho_1)(1-b\rho_2)}. \tag{18}$$

On the other hand, Eq. (15) readily gives

$$\rho'(z)=\frac{\rho_2-\rho_1}{D}\frac{1}{\cosh^2(2z/D)}, \tag{19}$$

and, following simple manipulations, the derivatives $\rho'(z)$ and $\rho''(z)$ can be expressed as the following functions of the local density:

$$\rho'(z)=\frac{4}{D}\frac{(\rho_2-\rho)(\rho-\rho_1)}{\rho_2-\rho_1}, \tag{20}$$

$$\rho''(z)=\frac{16}{D^2}\frac{(\rho_2-\rho)(\rho-\rho_1)(\rho_1+\rho_2-2\rho)}{(\rho_2-\rho_1)^2}. \tag{21}$$

We see again that the second derivative, $\rho''(z)$, of the mass density profile in Eq. (15), can be written in the form

$$\rho''(z)=A(\rho)/D^2, \tag{22}$$

where A is a function of the local mass density only:

$$A(\rho)=\frac{16(\rho_2-\rho)(\rho-\rho_1)(\rho_1+\rho_2-2\rho)}{(\rho_2-\rho_1)^2}. \tag{23}$$

Substitution of Eqs. (16) and (22) into Eq. (14) gives

$$mA(\rho)=D^2kTf(\rho), \tag{24}$$

which provides a connection between the temperature and the desirable width of the interface. Since, in the general case, Eq. (15) is only an approximate solution of Eq. (14) (for T close to T_c), which is valid locally within the interfacial region, we can set kT using the following least-square minimization procedure:

$$\min_{kT} \sum_{\{z_i\} \in \text{interface}} [mA(\rho^*(z_i)) - D^2 kT f(\rho^*(z_i))]^2, \quad (25)$$

where z_i is the coordinate of the position vector at the lattice site i, in the direction normal to the interface, and $\rho^*(z_i)$ provides linear interpolation between the vapor and liquid densities. In fact, this is equivalent to fitting the real density profile with a model function, like that given by Eq. (15). Hence, one can *prescribe the width* D, of the interface, in which case the thermal energy term should be obtained from

$$kT = \frac{m \sum_{\{z_i\} \in \text{interface}} A(\rho(z_i)) f(\rho(z_i))}{D^2 \sum_{\{z_i\} \in \text{interface}} f^2(\rho(z_i))}. \quad (26)$$

On the other hand, the van der Waals theory gives the following expression for the interfacial tension at a flat interface:

$$\sigma = m \int_{-\infty}^{\infty} \rho'^2(z) \mathrm{d}z. \quad (27)$$

Substitution of Eq. (19) into (27), followed by integration, yields the expression

$$m = \frac{3D\sigma}{2(\rho_2 - \rho_1)^2}. \quad (28)$$

Equations (26) and (28) allow the direct prescription of both the surface tension σ and the interface thickness D in the two-phase system of interest. Once the vapor and liquid densities ρ_1 and ρ_2, the surface tension σ, and the width D, are prescribed, one can calculate the value of the parameter m from Eq. (28) and the value of the thermal energy term kT from Eq. (26). The value of the constant b can be obtained by solving Eq. (6) numerically. Finally, the value of the constant a is obtained from Eq. (7).

III. IMPLEMENTATION OF FLOW CONDITIONS

Flow conditions can be imposed in the framework of this model through the action of either a constant pressure gradient or gravity. Thus, flow in the x direction, for instance, can be induced by modifying the local pressure according to

$$P = P_0(\rho, T) + \mathbf{x} \cdot \nabla P \quad \text{(pressure-gradient-driven flow)}, \quad (29)$$

or

$$P = P_0(\rho, T) - \rho \mathbf{g} \cdot \mathbf{x} \quad \text{(gravity-driven flow)}, \quad (30)$$

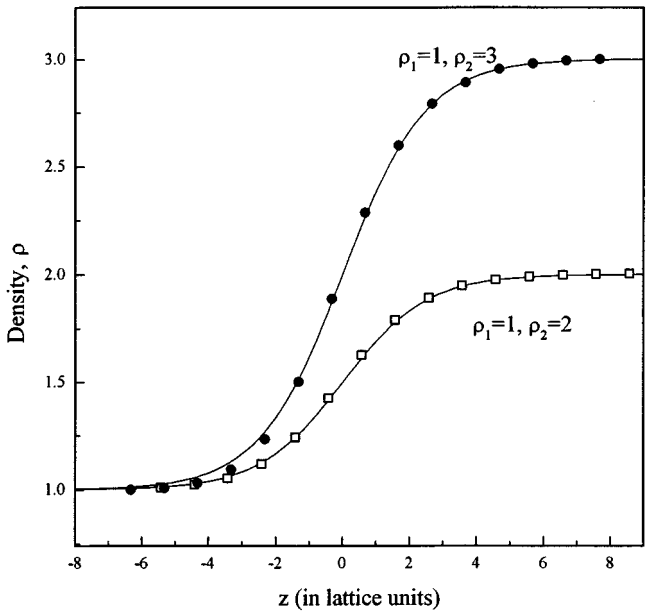

FIG. 2. Density profiles across a gas-liquid interface. Solid lines, Eq. (15); symbols, simulation results.

where $P_0(\rho, T)$ is the pressure given by the equation of state, $\mathbf{g}$ is the acceleration of gravity, and ∇P is the externally applied pressure gradient.

IV. RESULTS AND DISCUSSION

In this section we demonstrate the applicability of the aforementioned algorithms for prescribing fluid properties in the context of the lattice-Boltzmann model for nonideal fluids [16]. We also present two-phase equilibrium and flow simulation results in the absence of walls as well as in the interior of porous media.

The first test concerns the prescription of liquid and vapor densities using the approach described in Sec. II. The hexagonal lattice is initially populated with the equilibrium densities of the two phases separated by a flat interface. The lattice dimensions are 400×400. 2×10^5 sites are updated per second on an 8-cpu SGI machine. Periodic boundary conditions are imposed on the box walls. The local densities are allowed to evolve according to the lattice-Boltzmann model keeping the temperature constant. It was found that the system becomes completely equilibrated following 20,000 time steps, at which time the density profiles were recorded. By calculating the local density gradients after equilibration, the surface tension is calculated from Eq. (27). The minimization procedure for the temperature estimation converged quite rapidly; use of only five points in Eq. (26) yielded an error of only 0.2% in the estimation of the prevailing temperature. For both density ratio values, the calculated surface tension value is $\sigma = 0.99 \times 10^{-3}$, which compares very satisfactorily to the prescribed value ($\sigma = 1.00 \times 10^{-3}$). The density profiles are shown in Fig. 2. Again, the calculated values of the local density (marked points) are in excellent agreement with the values that are obtained from Eq. (15) (solid lines). However, it was found that when very

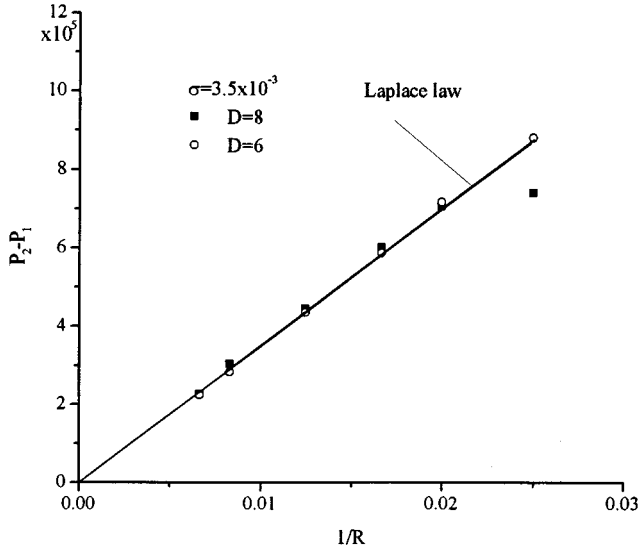

FIG. 3. Laplace law test for a 2D bubble. Solid line, Laplace law for prescribed value, $\sigma = 3.5 \times 10^{-3}$; symbols, simulation results for two values of the interface thickness D.

small density ratio values are used (<0.2) and a sharp interface ($D<1.5$) is desired, the error may become significant. This loss of accuracy is attributed to the violation of the assumption made in the analysis regarding the temperature of the two-phase system, namely, that the temperature is sufficiently close to the critical temperature of the substance under consideration (see Fig. 1). A further reason for this deviation is the inherent discretization errors of the lattice-Boltzmann simulation.

The second test examines the consistency of the lattice-Boltzmann approach with the Laplace law, when the prescription algorithms of Sec. II are adopted. Again, a

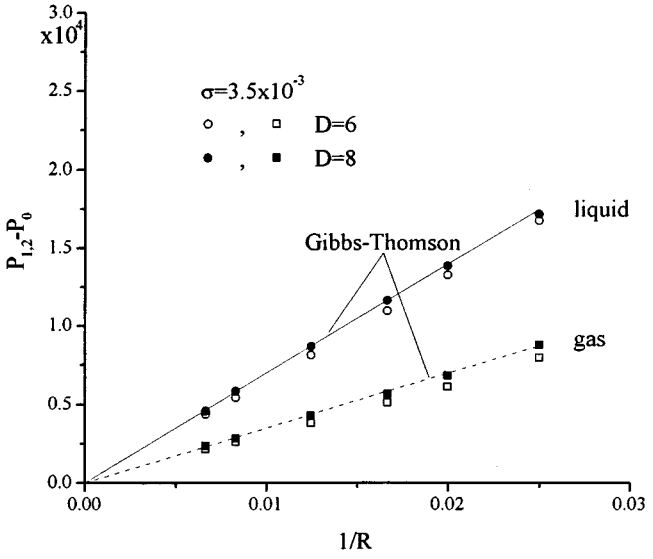

FIG. 4. Comparison of calculated liquid and gas pressure values (symbols) with the Gibbs-Thomson estimates (solid lines) for a liquid droplet. P_0 is the liquid and gas (common) pressure value for a flat interface.

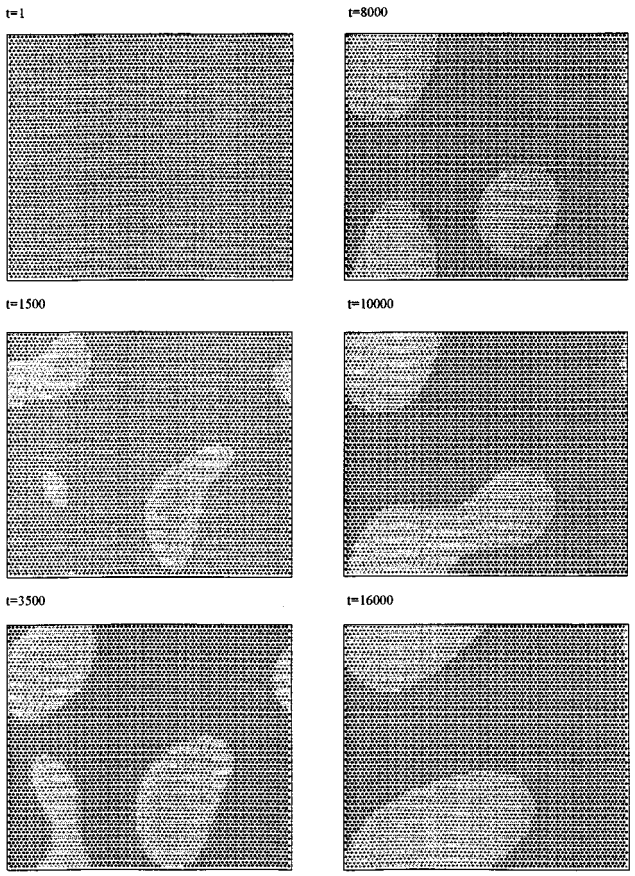

FIG. 5. Simulation of spinodal decomposition (t: time steps) $\rho_1 = 2.8$, $\rho_2 = 4.2$, $\sigma = 2.65 \times 10^{-3}$, $D = 3$, and $\nu_1 = \nu_2 = 0.7$.

400×400 hexagonal lattice is used, with periodic boundary conditions on the box walls. The formation of a 2D bubble is simulated under the action of a prescribed value of surface tension. The pressure difference across the vapor-liquid interface is calculated after 20,000 time steps, which were found necessary for equilibration. Figure 3 shows that the calculated pressure difference increases in an almost linear fashion with increasing curvature of the bubble for both values of interface thickness considered. Our calculations have shown that as the ratio of interface thickness to droplet radius becomes larger than about 0.2, significant deviation of the calculated capillary pressure value from the theoretical one (based on Laplace law) may develop. This critical value is, however, a function of the surface tension and the van der Waals constants for the same liquid and vapor densities.

A test of thermodynamic consistency of the model and prescription algorithms is presented in Fig. 4, where the differences $P_1 - P_0$ and $P_2 - P_0$ plotted against the droplet curvature. A 400×400 grid was used; the calculated values (symbols) refer to two different values of interface thickness, $D = 6$ and $D = 8$. The solid lines represent the theoretical estimates of the same quantities according to the Gibbs-Thomson equations:

$$P_1 = P_0 + \frac{\rho_1}{\rho_2 - \rho_1} \frac{\sigma}{R}, \tag{31a}$$

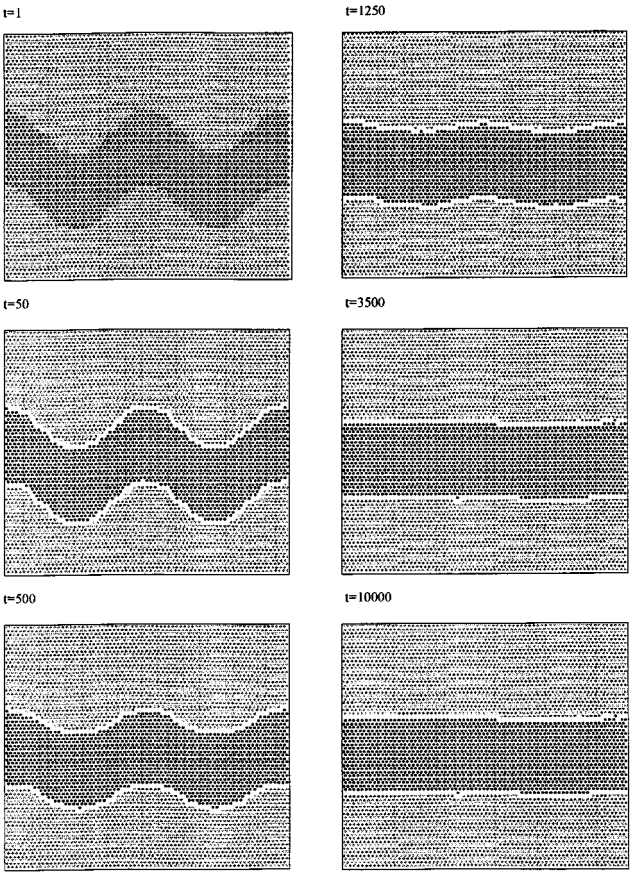

FIG. 6. Relaxation of liquid film initially in bending mode. $\rho_1=2.8$, $\rho_2=4.2$, $\sigma=2.65\times10^{-3}$, $D=5.3$, and $\nu_1=\nu_2=0.7$.

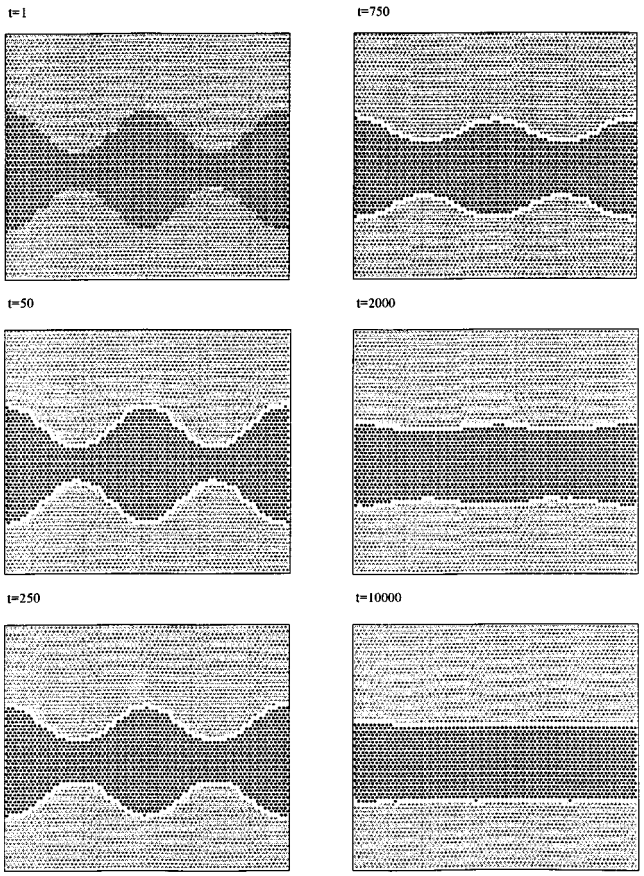

FIG. 7. Relaxation of liquid film initially in squeezing mode. $\rho_1=2.8$, $\rho_2=4.2$, $\sigma=2.65\times10^{-3}$, $D=5.3$, and $\nu_1=\nu_2=0.7$.

$$P_2=P_0+\left(1+\frac{\rho_1}{\rho_2-\rho_1}\right)\frac{\sigma}{R}. \tag{31b}$$

The agreement of the calculated values with the theoretical ones shown in Fig. 4 is quite satisfactory. To the best of the authors' knowledge no previous lattice scheme has reported this level of numerical agreement. Instead, correction factors had to be introduced into the Gibbs-Thomson equations in order for the calculated pressure values to comply with them (see, e.g., Ref. [11]).

Figure 5 shows the evolution of a system undergoing a phase transition. The equilibrium densities of the vapor and liquid phases are set to $\rho_1=2.8$ and $\rho_2=4.2$, respectively, and the kinematic viscosities to $\nu_1=\nu_2=0.7$. The surface tension is set to $\sigma=2.65\times10^{-3}$ and the effective width of the interface, D, to three lattice units. Periodic boundary conditions are imposed on a 70×70 hexagonal lattice, which is initially ''populated''with a uniform density, $\rho=3.62$. The initiation of the phase transition experiment is triggered by small fluctuations ($\pm1\%$) of the local density imposed at random positions throughout the lattice. The first discernible nuclei appear after about 800 time steps, and these grow progressively to droplets. The latter coalesce to larger droplets leading to the final separation state after 16,000 time steps.

Two-phase flow that is induced by interface relaxation is studied next. Figures 6 and 7 present snapshots taken during deformation of a liquid film subject to bending and squeezing, respectively. In both cases the interfaces relax to a flat film, causing flow within the film and in the surrounding vapor phase. It is estimated that similar relaxation times are required for both configurations (11,000 time steps), provided they share, initially, the same wavelength and amplitude.

Figure 8 shows different stages of a coalescence process, taking place between two liquid droplets. A vapor film, the thickness of which is smaller than the interface thickness prescribed for the experiment, initially separates the droplets. The density gradients in the interface region give rise to the development of the so-called Ostwald ''ripening'' phenomenon and lead to complete coalescence into a droplet of volume equal to the sum of the volumes of the original droplets.

The interaction between a liquid film and a liquid droplet is simulated in Figs. 9 and 10. Depending on the relative volumes of the two liquid bodies, different final configurations can be reached. In Fig. 9 the film disappears, giving rise to a droplet larger than the original one by an amount equal to the film volume. In Fig. 10 the film thickness increases by the droplet volume. The difference in the resulting configurations can be explained as follows. Because of the periodic boundary conditions imposed on the wall surfaces, there are two minima in the free energy of the system for a given volume ratio of the two phases. These minima correspond to two different equilibrium shapes of the interface, namely, *circular* (droplet) and *slab* (film). Depending on the volume ratio of the two phases, one of these minima is glo-

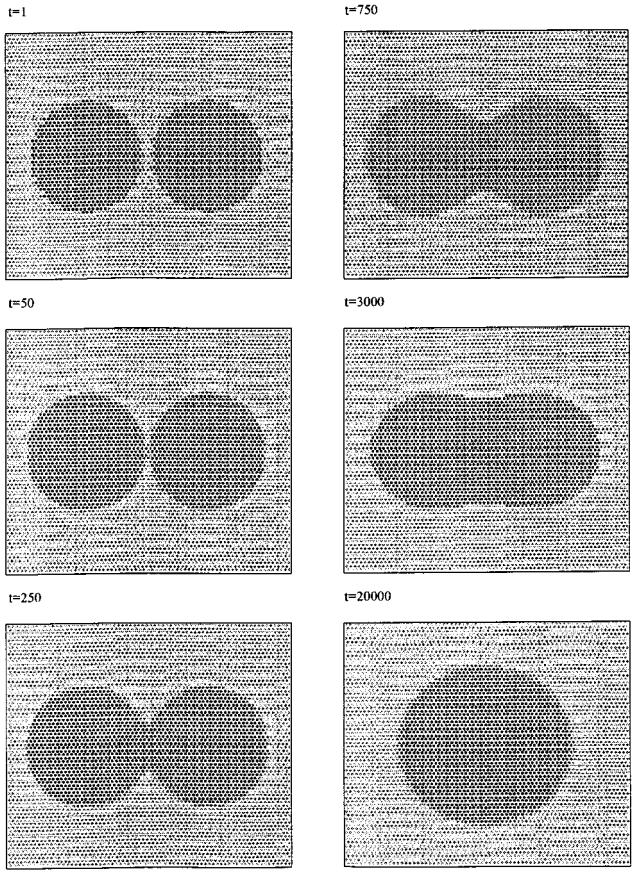

FIG. 8. Coalescence of 2D liquid droplets. $\rho_1=2.8$, $\rho_2=4.2$, $\sigma=2.65\times10^{-3}$, $D=5.3$, and $\nu_1=\nu_2=0.7$.

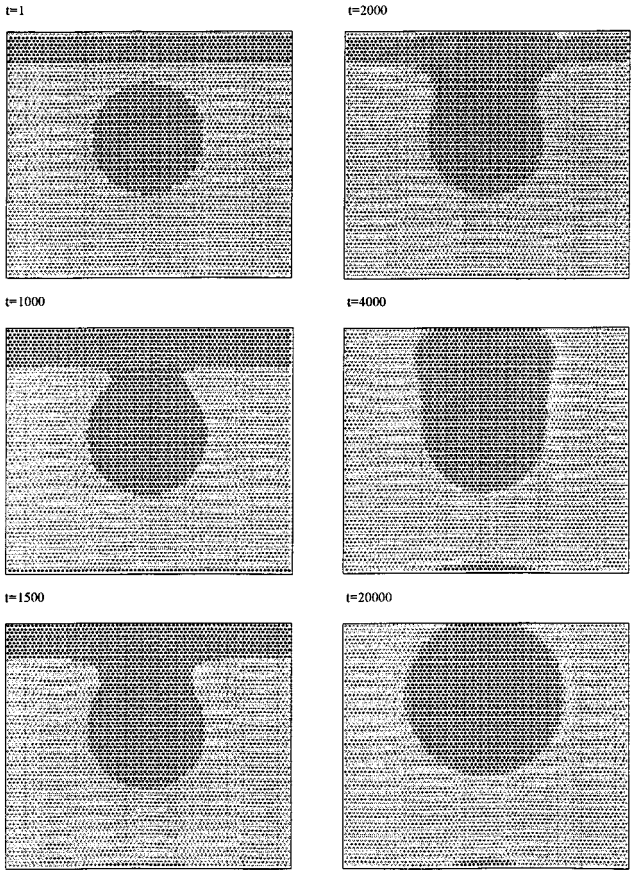

FIG. 9. Coalescence of thin liquid film with liquid droplet. $h/L=0.1$, $R/L=0.25$, $\rho_1=2.8$, $\rho_2=4.2$, $\sigma=2.65\times10^{-3}$, $D=5.3$, and $\nu_1=\nu_2=0.7$.

bal, whereas the other one is local. The values of the volume ratio in the two experiments are such that the global minimum of the free energy corresponds to a *circular interface* in the first case (Fig. 9) and a *flat interface* in the second one (Fig. 10). A simple calculation verifies this result. Consider a periodic $L\times L$ 2D lattice, a film of thickness h, and a droplet of radius R. If $\pi h/L+(\pi R/L)^2<1$, the circular geometry will be favored, because it provides smaller interface length compared to that of the slab (Fig. 9). In the opposite case, the final configuration will be that of slab geometry (Fig. 10). Thanks to space discretization and the fact that π is irrational, the case of equality in the above expression is impossible.

Figure 11 presents simulated snapshots of the motion of a deformable bubble in a straight channel with a solid barrier. The lattice is initially populated with the heavier phase (liquid) and a bubble is placed close to the left channel end. No-slip boundary conditions are imposed on the channel walls and on the barrier (see, e.g., Ref. [21]). Periodic boundary conditions are imposed on the two channel ends. In the first stage of the simulation, the bubble is given sufficient time (about 2000 time steps) to relax and adopt a circular shape; then, gravity-driven flow is imposed according to Eq. (30) with $g=2.5\times10^{-5}$ acting in the negative x direction. The Reynolds number is 0.5 and the surface tension is set to the value $\sigma=3.5\times10^{-3}$. It is interesting to note that the bubble follows a pathway that drives it through the upper opening, which is wider than the lower one by a single lattice unit and, consequently, presents a slightly smaller capillary resistance.

The two-phase flow simulator was also applied to the case of vapor displacement by liquid in a porous medium. The void space of the medium is represented as a collection of large pore bodies, called chambers, interconnected through narrow capillaries called throats. Such a representation has been repeatedly proved satisfactory for a variety of practical materials used in chemical, physical, and biological processes, such as catalysts, packed beds, oil reservoirs, macromolecule coils, etc. [22–27]. The pore network is initially filled with vapor and at $t=0$ a liquid phase is injected from the left face of the working sample (Fig. 12). The liquid displaces the vapor at a very large capillary number (Ca $=10^{-2}$) and leads, eventually, to a very efficient sweep. No preferential wetting is imposed in this experiment. However, introduction of wettability in the system may lead to drastic changes in the displacement process. The desired wettability conditions can be implemented by assigning a prescribed profile of chemical potential $\mu_w(\mathbf{r})$ to the pore walls [16] or, equivalently, by assigning a certain profile of equilibrium density to the boundary sites $\rho_w(\mathbf{r})$ that corresponds, pointwise, to $\mu_w(\mathbf{r})$ according to Eq. (4). In this fashion, the simulation of flooding processes in actual hydrocarbon fields with nonuniform wettability can be decisively facilitated. Figure 13 shows four snapshots of an imbibition simulation, where the liquid phase is assumed to wet the pore surface

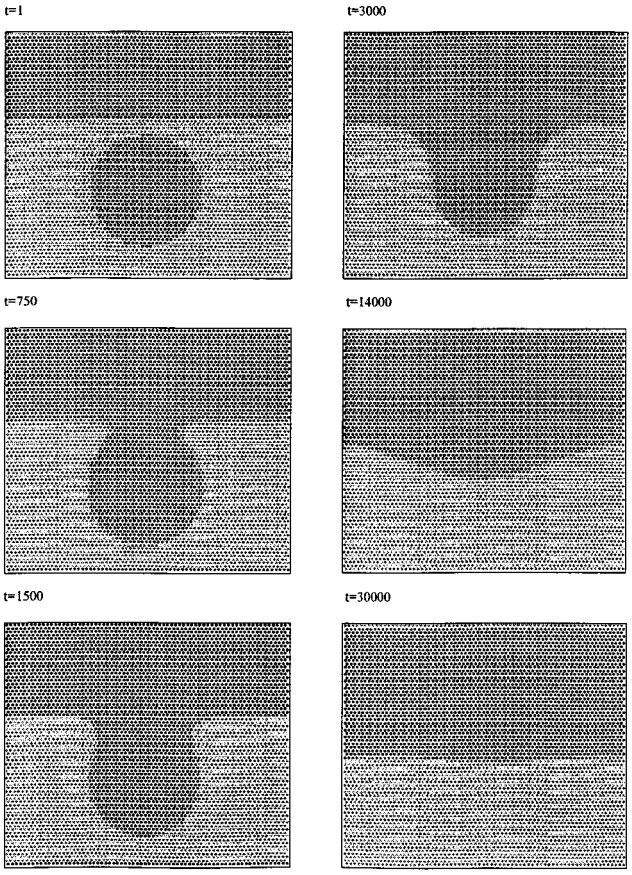

FIG. 10. Coalescence of thick liquid film with liquid droplet. $h/L=0.35$, $R/L=0.25$, $\rho_1=2.8$, $\rho_2=4.2$, $\sigma=2.65\times10^{-3}$, $D=5.3$, and $\nu_1=\nu_2=0.7$.

strongly, forming a thin liquid film along the pore walls. Breakthrough is attained very quickly in this experiment; the liquid phase advances through the pore network through, mainly, film flow resulting in poor sweeping efficiency. The

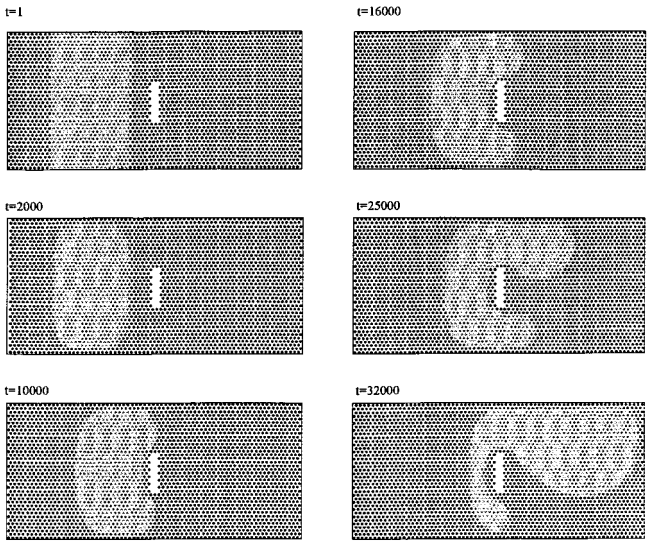

FIG. 11. Motion of a deformable 2D bubble in a channel with a solid obstacle. $\rho_1=2.5$, $\rho_2=4.2$, $\sigma=3.5\times10^{-3}$, $D=3$, and $\nu_1=\nu_2=0.7$.

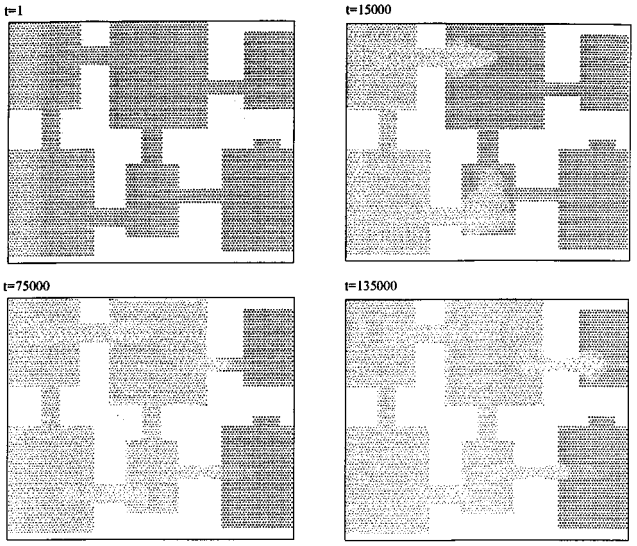

FIG. 12. Immiscible displacement of vapor by liquid in a chamber-and-throat pore network with no preferential wettability. $\rho_1=1$, $\rho_2=2$, $\sigma=10^{-4}$, $D=3$, and $\nu_1=\nu_2=0.7$.

gradual increase of the film thickness causes, eventually, snap-off at pore throats and entrapment of a large vapor quantity in pore chambers (see, also, Refs. [1,2]). Continued application of an external pressure gradient causes, eventually, condensation of the trapped vapor, progressively from left to right and from smaller to larger pore chambers.

V. CONCLUDING REMARKS

An algorithm for the prescription of equilibrium fluid properties in lattice-Boltzmann simulations of two-phase systems is presented in this work. The algorithm uses elements from the van der Waals and mean-field theories for

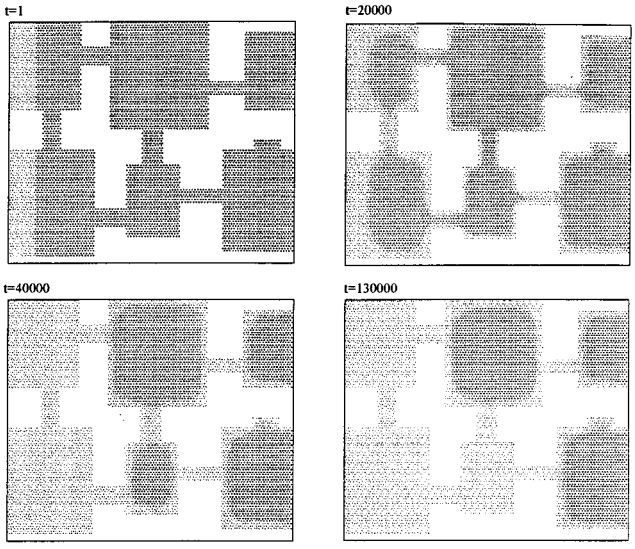

FIG. 13. Immiscible displacement of vapor by liquid in a chamber-and-throat pore network with the liquid wetting the solid walls. $\rho_1=1$, $\rho_2=2$, $\rho_w=1.97$, $\sigma=10^{-4}$, $D=3$, and $\nu_1=\nu_2=0.7$.

liquid-vapor systems and provides useful expressions for the prescription of equilibrium densities, kinematic viscosities, and interfacial tension. Several simulation tests were run using the pioneering lattice-Boltzmann model for nonideal gases by Swift, Osborn, and Yoemans [16]. The algorithm proved very efficient and accurate in prescribing the aforementioned fluid properties, provided that the thickness of the interface between the vapor and the liquid is larger than a critical value (typically $\geqslant 1.5$ lattice units).

It was found that the Gibbs-Thomson equations are satisfied with good accuracy by our simulation results for a liquid droplet at equilibrium. Such an agreement between calculated and theoretical pressure values is achieved for the first time by a lattice model and provides an additional argument in support of not only the consistency of the model with thermodynamics, but also the prescription algorithm that was introduced in this work.

The lattice-Boltzmann simulator was applied to two-phase flow problems in simple geometries and in pore networks. It was found that the simulator can predict several two-phase flow phenomena of critical significance in displacement applications, such as formation of advancing wetting film and early breakthrough under strong wettability conditions, film growth and snap off in throats, vapor condensation in pore chambers, and wettability-dependent sweeping efficiency of waterfloods.

Some thoughts regarding Galilean invariance are in order. Possible lack of Galilean invariance in the nonideal lattice-Boltzmann model may be due to the appearance in the viscous term of the Navier-Stokes equation of a density-dependent quantity, namely, the derivative of the pressure with respect to density [19]. However, careful analysis of this quantity has shown that it can be rendered negligible, especially in the near-critical region, provided that the appropriate choices of van der Waals constants and fluid densities are made. Moreover, under typical field conditions in hydrocarbon recovery and land contamination applications, the pertinent capillary number is sufficiently low (10^{-10}–10^{-8}) for this term to be insignificant.

ACKNOWLEDGMENTS

This work was supported by EC, Project No. BRE2-CT92-0191, and by the Institute of Chemical Engineering and High Temperature Chemical Processes. Thanks are due to A. Baxevanis for his contribution to the development of the CA graphics.

[1] O. Vizika and A. C. Payatakes, PCH Physicochem. Hydrodyn. **11**, 187 (1989).
[2] O. Vizika, D. G. Avraam, and A. C. Payatakes, J. Colloid Interface Sci. **165**, 386 (1994).
[3] D. G. Avraam and A. C. Payatakes, J. Fluid Mech. **293**, 207 (1995).
[4] R. Benzi, S. Succi, and M. Vergassola, Phys. Rep. **222**, 145 (1992).
[5] S. Chen, Z. Wang, X. Shan, and G. Doolen, J. Stat. Phys. **68**, 379 (1992).
[6] D. Rothman and J. M. Keller, J. Stat. Phys. **52**, 119 (1988).
[7] A. K. Gustensen, D. H. Rothman, S. Zaleski, and G. Zanetti, Phys. Rev. A **43**, 4320 (1991); A. K. Gunstensen and D. H. Rothman, Europhys. Lett. **18**, 157 (1992).
[8] D. Grunau, S. Chen, and K. Eggert, Phys. Fluids A **5**, 2557 (1993).
[9] C. Appert and S. Zaleski, Phys. Rev. Lett. **64**, 1 (1990).
[10] C. Appert, D. H. Rothman, and S. Zaleski, Physica D **47**, 85 (1991).
[11] C. Appert and S. Zaleski, J. Phys. II **3**, 309 (1993).
[12] C. Appert, D. d'Humieres, and S. Zaleski, C. R. Acad. Sci., Ser. II: Mec., Phys., Chim., Sci. Terre Univers **316**, 569 (1993).
[13] H. Chen, S. Chen, G. Doolen, Y. C. Lee, and H. Rose, Phys. Rev. A **40**, 2850 (1989).
[14] X. Shan and H. Chen, Phys. Rev. E **47**, 1815 (1993).
[15] X. Shan and H. Chen, Phys. Rev. E **49**, 2941 (1994); X. Shan and G. Doolen, J. Stat. Phys. **81**, 379 (1995).
[16] M. R. Swift, W. R. Osborn, and J. M. Yeomans, Phys. Rev. Lett. **75**, 830 (1995).
[17] E. Orlandini, M. R. Swift, and J. M. Yeomans, Europhys. Lett. **32**, 463 (1995).
[18] W. R. Osborn, E. Orlandini, M. R. Swift, J. M. Yeomans, and J. R. Banavar, Phys. Rev. Lett. **75**, 830 (1995).
[19] M. R. Swift, E. Orlandini, W. R. Osborn, and J. M. Yeomans, Phys. Rev. E **54**, 5041 (1996).
[20] J. W. Cahn and J. E. Hilliard, J. Chem. Phys. **28**, 258 (1958). J. S. Rowlinson and B. Widom, *Molecular Theory of Capillarity* (Clarendon, Oxford, 1982).
[21] R. Cornubert, D. d'Humières, and D. Levermore, Physica D **47**, 241 (1991).
[22] M. Yanuka, F. A. L. Dullien, and D. E. Erlick, J. Colloid Interface Sci. **112**, 24 (1986).
[23] A. C. Payatakes, C. Tien, and R. M. Turian, AIChE. J. **19**, 58 (1973); **19**, 67 (1973).
[24] V. N. Burganos, C. A. Paraskeva, and A. C. Payatakes, AIChE. J. **41**, 272 (1995).
[25] J. Koplik and T. J. Lasseter, SPE Paper No. 11014 (1982).
[26] Y. Li, W. G. Laidlaw, and N. C. Wardlaw, Adv. Colloid Interface Sci. **26**, 1 (1986).
[27] J. D. Chatzis and F. A. L. Dullien, Int. J. Chem. Eng. **25**, 47 (1985).